^{27}Al^{+} Quantum-Logic Clock with a Systematic Uncertainty below 10^{-18}

S. M. Brewer, J.-S. Chen, A. M. Hankin, E. R. Clements, C. W. Chou, D. J. Wineland, D. B. Hume, and D. R. Leibrandt

Phys. Rev. Lett. **123**, 033201 — Published 15 July 2019

DOI: 10.1103/PhysRevLett.123.033201

An $^{27}Al^+$ quantum-logic clock with systematic uncertainty below 10^{-18}

S. M. Brewer,[1,2,*] J.-S. Chen,[1,2,†] A. M. Hankin,[1,2,‡] E. R. Clements,[1,2]
C. W. Chou,[1] D. J. Wineland,[1,2,3] D. B. Hume,[1] and D. R. Leibrandt[1,2,§]

[1] *Time and Frequency Division, National Institute of Standards and Technology, Boulder, CO 80305*
[2] *Department of Physics, University of Colorado, Boulder, CO 80309*
[3] *Department of Physics, University of Oregon, Eugene, OR 97403*

(Dated: June 3, 2019)

We describe an optical atomic clock based on quantum-logic spectroscopy of the $^1S_0 \leftrightarrow {}^3P_0$ transition in $^{27}Al^+$ with a systematic uncertainty of 9.4×10^{-19} and a frequency stability of $1.2 \times 10^{-15}/\sqrt{\tau}$. A $^{25}Mg^+$ ion is simultaneously trapped with the $^{27}Al^+$ ion and used for sympathetic cooling and state readout. Improvements in a new trap have led to reduced secular motion heating, compared to previous $^{27}Al^+$ clocks, enabling clock operation with ion secular motion near the three-dimensional ground state. Operating the clock with a lower trap drive frequency has reduced excess micromotion compared to previous $^{27}Al^+$ clocks. Both of these improvements have led to a reduced time-dilation shift uncertainty. Other systematic uncertainties including those due to blackbody radiation and the second-order Zeeman effect have also been reduced.

In 1973, Hans Dehmelt proposed a frequency standard based on a single trapped ion, dubbed the "mono-ion oscillator", based on the $^1S_0 \leftrightarrow {}^3P_0$ transition in Tl^+ [1, 2]. Sideband cooling was later added to this proposal [3] and, in 1982, the proposal was expanded to include B^+, Al^+, Ga^+ and In^+ [4]. In [4] the possibility of a clock with a fractional frequency uncertainty of 10^{-18} was first discussed, setting the stage for a series of experiments that continue to push the limits of measurement science. For trapped-ion systems, the systematic uncertainty was predicted to be limited by uncertainty in second-order Doppler (time-dilation) shifts due to the ion motion.

At this level of systematic uncertainty it is possible to measure clock frequency ratios that could lead to improved limits on the time-variation of fundamental constants, investigate dark matter composition, and probe physics beyond the standard model [5]. Additionally, systematic uncertainty of 10^{-18} is one of the criteria in the roadmap for a possible redefinition of the SI second based on an optical frequency standard [6]. Furthermore, since the current techniques used for the characterization of the Earth's geoid are limited at a level corresponding to height differences of a few cm corresponding to gravitational redshifts of a few times 10^{-18} [7], it is possible to use optical clocks at this level to improve knowledge of the geoid [8].

Since the original optical frequency standard proposals, significant experimental progress has been made in both systematic uncertainty and stability [8–14]. However, the systematic uncertainty of some of the highest performance trapped-ion clocks has been limited by Doppler shifts [9, 12, 15] that arise from ion trap imperfections that cause excess micromotion (EMM) and thermal (secular) motion.

Here, we report the systematic uncertainty evaluation of an optical atomic clock based on quantum-logic spectroscopy of $^{27}Al^+$ with a fractional frequency uncertainty of $\Delta\nu/\nu = 9.4 \times 10^{-19}$, which is the lowest systematic uncertainty reported for any clock to date. This is achieved by operating the clock close to the three-dimensional (3D) motional ground state utilizing a new trap design that reduces secular motion heating and with lower trap drive and secular frequencies to reduce EMM compared to previous $^{27}Al^+$ systems, resulting in an order-of-magnitude reduction in uncertainty due to Doppler shifts [9, 15]. In addition, we report a measurement of the clock stability, $\sigma(\tau) = 1.2 \times 10^{-15}/\sqrt{\tau}$.

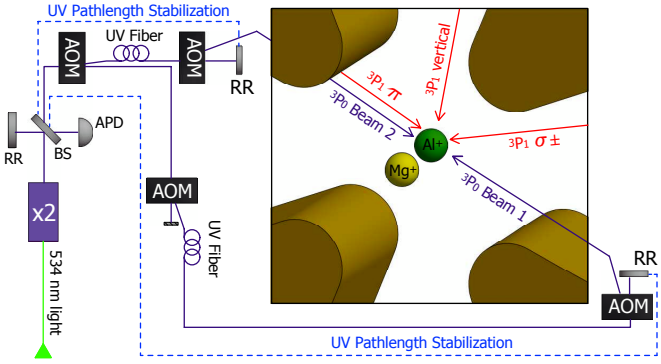

FIG. 1. Simplified schematic of the quantum-logic clock experimental setup. A frequency-quadrupled Yb-doped fiber laser is locked to the $^1S_0 \leftrightarrow {}^3P_0$ transition ($\lambda \simeq 267$ nm) by alternating the probe direction between two counter-propagating laser beams (shown in violet). An enlarged view of the trapping region is shown on the right. Three nominally orthogonal beams used for micromotion measurements are shown in red. Acousto-optic modulator (AOM); beam splitter (BS); retro-reflector (RR); frequency doubling stage (x2).

The experimental setup, including the trap design and ground-state cooling (GSC) sequence, is described in detail elsewhere [16–18]. A simplified schematic of the laser beams used to address $^{27}Al^+$ is shown in Fig. 1. The trap operates with a radiofrequency (RF) drive frequency of $\Omega_{RF}/2\pi = 40.72$ MHz and a differential drive amplitude of approximately $\pm$ 30 V. The radial secular frequen-

cies (motion perpendicular to the trap axis) of a single $^{25}Mg^+$ ion are $\omega_x/2\pi \approx 3.4$ MHz and $\omega_y/2\pi \approx 4.0$ MHz and the axial frequency is $\omega_z/2\pi \approx 1.5$ MHz. The clock operation sequence begins with preparation of the $^{27}Al^+$ state in either $|^1S_0, m_F = \pm 5/2\rangle$ by optical pumping on the $^1S_0 \leftrightarrow {}^3P_1$ transition. Next, the $^{25}Mg^+/^{27}Al^+$ pair is cooled to near the 3D motional ground state using 1 ms of far-detuned ($\Delta/2\pi = -415$ MHz) laser cooling, 2 ms of Doppler cooling ($\Delta/2\pi = -20$ MHz), and ≈ 12 ms of pulsed Raman sideband cooling applied to the $^{25}Mg^+$ ion [16–18]. Finally, a 150 ms clock interrogation pulse is applied to the $^{27}Al^+$ ion, followed by quantum-logic readout [25, 26]. The clock is operated using Rabi spectroscopy with a Fourier-limited linewidth and ≈ 70 % contrast (Fig. 3).

The $^{27}Al^+$ ion is interrogated alternately on the $|^1S_0, m_F = \pm 5/2\rangle \leftrightarrow |^3P_0, m_F = \pm 5/2\rangle$ transitions to generate a clock frequency that is to first-order insensitive to external magnetic fields [27]. In addition to clock interrogation, auxiliary operations are interleaved to stabilize the orientation of the ion pair, track the $^1S_0 \leftrightarrow {}^3P_1$ frequency, and compensate excess micromotion (EMM) in real-time. The clock duty cycle is ≈ 50 %, with ≈ 45 % devoted to cooling, state preparation, and readout and ≈ 5 % for auxiliary operations.

Systematic frequency shifts and associated uncertainties are listed in Table I. In previous $^{27}Al^+$ clocks, the dominant systematic uncertainty was due to EMM [9, 15]. To evaluate the EMM shift and uncertainty we use the resolved-sideband technique [28, 29]. The time-dilation shift $\Delta\nu/\nu$ due to EMM measured in a particular direction is given by

$$\frac{\Delta\nu}{\nu} = -\frac{\langle v_{EMM}^2\rangle}{2c^2} = -\left(\frac{\Omega_{RF}}{\omega_L}\right)^2 \left(\frac{\Omega_{EMM}^{(\pm 1)}}{\Omega^{(0)}}\right)^2, \qquad (1)$$

where v_{EMM} is the velocity of the ion in the direction of the probe beam k-vector, c is the speed of light, $\omega_L = 2\pi c/\lambda_L$ is the probe laser frequency, and $\Omega^{(0)}(\Omega_{EMM}^{(\pm 1)})$ is the carrier (micromotion sideband) Rabi rate of the atomic transition. In addition to the time-dilation shift, there exists an AC Stark shift due to the trap RF drive field. The time-dilation shift and the RF drive AC Stark shift add to give the total frequency shift due to EMM [9],

$$\frac{\Delta\nu}{\nu} = -\frac{\langle v_{EMM}^2\rangle}{2c^2}\left[1 + \left(\frac{\Omega_{RF}/2\pi}{400\text{ MHz}}\right)^2\right], \qquad (2)$$

where the second term contributes approximately 1 % to the total shift at $\Omega_{RF}/2\pi = 40.72$ MHz.

Measurements of the EMM were made on the $^{27}Al^+$ ion using the $^1S_0 \leftrightarrow {}^3P_1$ transition at $\lambda_L = 267$ nm, with three nearly orthogonal beams (see Fig. 1). Figures 2(a) and 2(b) show the sum of the EMM shifts measured along the three probe directions, $\hat{k}_i$, given by $\sum_{\hat{k}_i} (\Delta\nu/\nu)_{EMM,\hat{k}_i}$. The EMM shift has been observed to be stable during clock operation both long term (Fig. 2(a)) and over the course of a day (Fig. 2(b)) when compensated in real-time. Based on these measurements, a histogram of possible time-dilation shifts (Fig. 2(c)) has been generated using a Monte-Carlo approach, which accounts for non-orthogonality of the probe beams and includes the statistical spread in the EMM measurements, uncertainty in $\vec{k}$ of the $^{27}Al^+$ $^3P_1$ beams, and ambiguity in the relative phase of the EMM components [18]. These results, combined with additional systematic uncertainties including the sampling of intrinsic micromotion [18], indicate an averaged EMM-induced frequency shift of $\Delta\nu/\nu = -(45.8 \pm 5.9) \times 10^{-19}$.

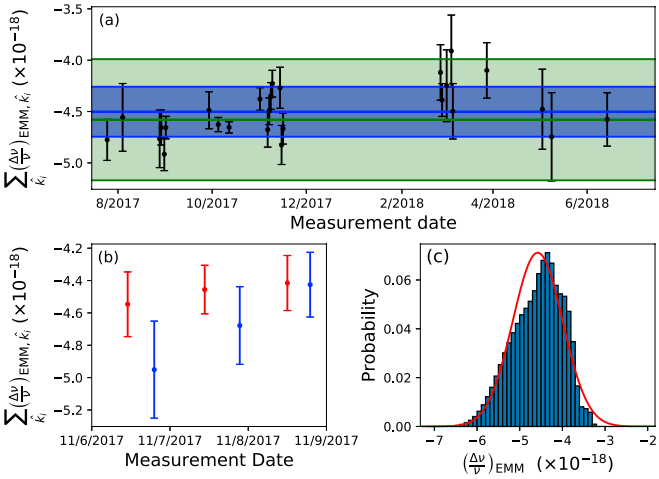

FIG. 2. Excess micromotion (EMM) shift evaluation. (a) The sum of the EMM frequency shifts (black points) measured along three nearly orthogonal probe directions from August 2017 to June 2018, with the average and standard deviation (blue line and band). (b) Sample of EMM measurements on three consecutive days. Red points are data taken immediately after initial EMM compensation and blue points are data taken after ≈ 12 hours of clock operation with interleaved micromotion compensation servos. (c) Histogram of possible total EMM shifts consistent with the measurements generated by a Monte-Carlo analysis accounting for non-orthogonality of the probe directions and assuming the worst-case scenario of either 0 or π phase between ion motion along these directions. The total EMM shift of $\Delta\nu/\nu = -(45.8 \pm 5.9) \times 10^{-19}$ is given by the mean and standard deviation of the calculated distribution and shown in (a) (green line and band). For reference, the red line shown in (c) is a normal (Gaussian) distribution with the same mean and standard deviation.

To mitigate the first-order Doppler shift due to motion of the ion that is correlated with the interrogation cycle, the clock transition is alternately interrogated with two laser beams that are approximately counterpropagating. Both beams are switched on during every probe cycle, with one of the beams detuned by 100 kHz from the transition so as to interact negligibly with the ion. Under these conditions, we expect that any stray electric

fields caused by photo-electrons generated by the clock laser light will be uncorrelated with the probe direction. Charging of surfaces inside the vacuum chamber due to 280 nm cooling light applied before the clock interrogation can also lead to time-dependent stray electric fields which cause ion motion. We observe an average first-order Doppler shift of $|\Delta\nu/\nu| = 4.6 \times 10^{-17}$, by comparing the center-frequency offset between the two opposing probe directions, as shown in Fig. 3(a).

For exactly counterpropagating beams and identical (but frequency shifted) lineshapes for the two probe directions, the first-order Doppler shift does not shift the clock frequency. If the spectroscopy lineshapes are different due to unequal intensity or phase noise on the two beams, the gain of the clock servo error signal will be different for the two probe directions. For servo algorithms in which the two directions are probed with the same laser frequency, as used in previous $^{27}Al^+$ clocks and shown in Fig. 3(a), this causes the output of the servo to be pulled closer to the probe direction that has higher contrast. To eliminate this as a potential source of systematic uncertainty, we use a clock servo algorithm in which the resonance frequencies of the two probe directions are tracked independently, and the servo synthesizes the mean of these frequencies as its output, shown in Fig. 3(b). We have verified numerically that the servo error of our first-order Doppler tracking servo is much less than the statistical clock instability for all measurement times > 100 s.

For perfectly counterpropagating probe beams, ion motion in any direction is exactly cancelled and does not contribute a systematic shift to the clock frequency. However, in the case of misalignment of the two beams, the Doppler shift due to motion along the bisector of their k-vectors is not suppressed. The two counterpropagating beams originate from UV fibers and are mode-matched on either side of the vacuum chamber to give approximately 60 % transmission through each opposing fiber. This contrains the angle between the wavefronts of the two clock beams at the location of the ion to be ≤ 3 mrad. We impose a bound on the maximum possible ion velocity that is consistent with EMM measurements made of the ion displacement at various times during the clock interrogation sequence (Fig. 3(c)). From the average radial mode frequency and the EMM amplitude we deduce the average ion displacement away from the fully compensated location and corresponding speed [18]. Based on this velocity constraint, we assign a first-order Doppler shift and uncertainty of $\Delta\nu/\nu = (0.0 \pm 2.2) \times 10^{-19}$.

The clock is operated with a bias magnetic field $B \approx 0.12$ mT. The quadratic Zeeman shift is given by $\Delta\nu/\nu = C_2\langle B^2\rangle$, where C_2 is the quadratic Zeeman coefficient and $\langle B^2\rangle = \langle B_{DC}\rangle^2 + \langle B_{AC}^2\rangle$ [9, 15]. Here B_{DC} is the static magnetic field measured in real-time and B_{AC} is constrained based on microwave frequency measurements made on the $^{25}Mg^+$ ion as well as the

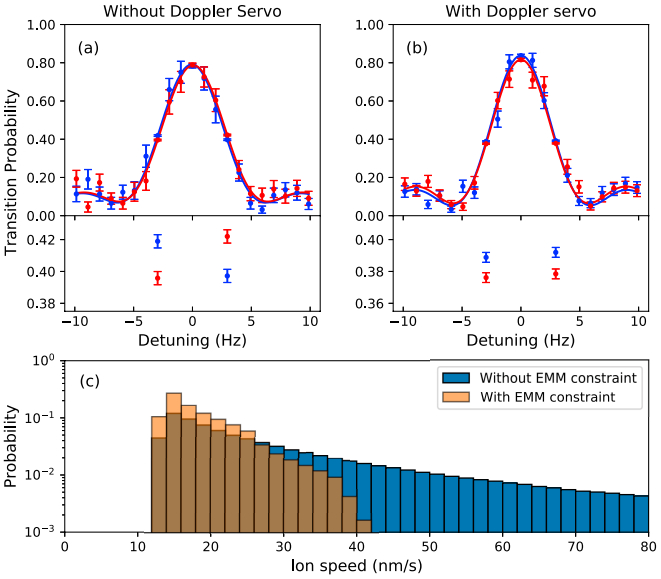

FIG. 3. First-order Doppler shift characterization. (a) Clock transition lineshapes for the two opposing probe directions (red and blue points) measured during clock operation without a first-order Doppler servo. Solid lines show fits to a Rabi lineshape. The zoomed in view shows that the transition probabilities at the probe frequencies used for the frequency lock are not balanced for each direction individually, indicating a non-zero first-order Doppler shift. (b) Similar data taken while running the first-order Doppler servo, with balanced transition probabilities at the lock points. (c) Distribution of possible ion speeds based on the measured first-order Doppler shift with and without an additional velocity constraint from EMM measurements.

uncertainty in the hyperfine constant A_{hfs} [30]. We have recently made improved measurements of both C_2 and A_{hfs} that are presented elsewhere [31]. The mean quadratic Zeeman shift for a day of operation is $\Delta\nu/\nu = -(9241.8 \pm 3.7) \times 10^{-19}$, where the exact value of the shift depends on the measured B_{DC}, but the uncertainty is not affected at the stated level of precision.

To reduce the frequency shift and uncertainty due to secular motion, the clock is operated close to the 3D motional ground state [16, 17]. The sideband cooling sequence is chosen to ensure at least 90 % of the remaining kinetic energy after Doppler cooling is removed [17]. The characterization of the energy after sideband cooling is accomplished by comparing a numerical simulation of the cooling dynamics with experimental measurements of the ion temperature [16]. The average occupation numbers of each motional mode estimated in [18] are used to calculate the time-dilation shift due to secular motion. At a clock interrogation time t_i, the fractional time-dilation shift due to secular motion is

$$\frac{\Delta\nu}{\nu} = \sum_p \left(\frac{\Delta\nu_p}{\nu}\right)\left[\left(\frac{1}{2} + \bar{n}_{p,0}\right) + \frac{1}{2}\dot{\bar{n}}_p\, t_i\right], \qquad (3)$$

where $(\Delta\nu_p/\nu)$ is the fractional time-dilation shift per

quantum of motion in a particular secular mode p, and $\bar{n}_{p,0}$ and $\dot{\bar{n}}_p$ are the average occupation number after cooling and the heating rate, respectively. The heating rate of each mode is measured using sideband thermometry [32, 33] and the results are summarized in [18]. For 150 ms clock interrogation time, the time-dilation shift due to secular motion is $\Delta\nu/\nu = -(17.3 \pm 2.9) \times 10^{-19}$.

The $^{27}Al^+$ clock is operated in an apparatus held near room temperature (≈ 295 K) and the presence of blackbody radiation (BBR) leads to an AC Stark shift on the clock transition. The clock frequency shift due to BBR depends on the sensitivity of the transition to thermal radiation, determined largely by the static differential polarizability, $\Delta\alpha_{clock}(0) = (7.02 \pm 0.95) \times 10^{-42}\mathrm{Jm}^2/\mathrm{V}^2$, and the temperature of the BBR at the position of the ion, T_{BBR} [18, 34]. For an uncertainty in T_{BBR} below 9 K, the uncertainty in $\Delta\alpha_{clock}(0)$ is the dominant uncertainty in the BBR shift evaluation. The temperature environment is characterized using seven thermocouple sensors; three located on the trap wafer and support structure and four located on the surrounding vacuum chamber [18]. These measurements constrain the temperature at the ion to be $T_{\mathrm{BBR}} = (294.8 \pm 2.7)$ K. The corresponding BBR induced frequency shift is evaluated as $\Delta\nu/\nu = -(30.5 \pm 4.2) \times 10^{-19}$.

Collisions of the $^{25}Mg^+/^{27}Al^+$ ion pair with background gas molecules cause both clock phase shifts and secular motion heating. Here, we summarize the background gas collision shift and uncertainty; details are presented in [35]. We measure the pressure of H_2 background gas at the position of the ions to be $(3.8 \pm 1.9) \times 10^{-8}$ Pa by monitoring the rate of collisions that cause the two ions to swap positions. Collisions of H_2 with either ion excite the secular motion into a non-thermal distribution with a tail extending out to near room temperature. This high energy tail is too small to detect with sideband thermometry heating rate measurements, but Monte-Carlo simulations of the clock interrogation indicate that it contributes a time-dilation shift $\Delta\nu/\nu = -0.6(^{+0.6}_{-0.3}) \times 10^{-19}$ which for bookkeeping purposes we do not include in our secular motion shift. When H_2 collides with $^{27}Al^+$ during the Rabi interrogation, the phase of the $^{27}Al^+$ superposition state is shifted, resulting in a spectroscopic frequency shift. Since the magnitude of this phase shift is unknown for $H_2/^{27}Al^+$ collisions, we bound the collisional frequency shift by assuming the worst case $\pm\pi/2$ phase shift for Langevin spiraling collisions that penetrate the angular momentum barrier. In this way, we constrain the collision shift to be $\Delta\nu/\nu = -(0.6 \pm 2.4) \times 10^{-19}$.

TABLE I. Fractional frequency shifts ($\Delta\nu/\nu$) and associated systematic uncertainties for the $^{27}Al^+$ quantum-logic clock.

Effect	Shift (10^{-19})	Uncertainty (10^{-19})
Excess micromotion	-45.8	5.9
Blackbody radiation	-30.5	4.2
Quadratic Zeeman	-9241.8	3.7
Secular motion	-17.3	2.9
Background gas collisions	-0.6	2.4
First-order Doppler	0	2.2
Clock laser Stark	0	2.0
AOM phase chirp	0	< 1
Electric quadrupole	0	< 1
Total	-9336.0	9.4

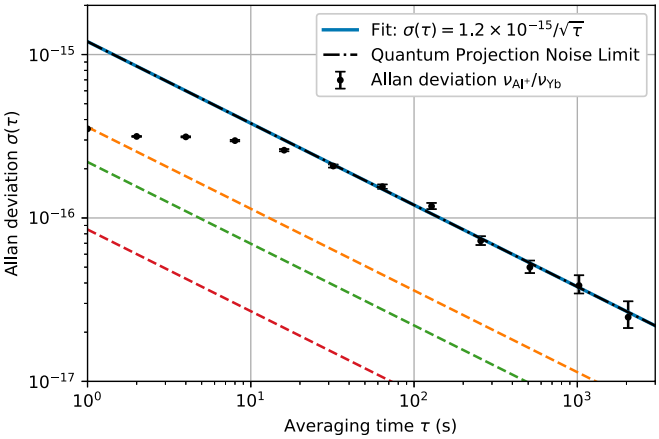

FIG. 4. Allan deviation of the frequency ratio $\nu_{\mathrm{Al}^+}/\nu_{\mathrm{Yb}}$ measured over $\approx 23,000$ s. The asymptote is fit to extract a frequency stability of $\sigma(\tau) = 1.2 \times 10^{-15}/\sqrt{\tau}$, where τ is the averaging time in seconds. Anticipated stabilities for a correlation spectroscopy comparison of two single-ion $^{27}Al^+$ clocks [39] (orange), a single $^{27}Al^+$ mixed-species correlation comparison [40] (green), and a single $^{27}Al^+$ ion clock operated using Rabi spectroscopy at the interrogation time of 20.6 s, equal to the excited state lifetime (red) are also shown.

A possible AC stark shift due to the clock probe beams has previously been investigated [9] and for the operating conditions used here, this leads to a clock laser induced AC stark shift of $\Delta\nu/\nu = (0.0 \pm 2.0) \times 10^{-19}$. Other possible frequency shifts include those due to a phase chirp in the clock beam AOMs and an electric quadrupole shift due to the (static) axial trapping potential. Uncertainties due to these shifts have been bounded below 10^{-19} [36].

The $^{27}Al^+$ clock stability, measured by comparing with a Yb lattice clock at NIST, is shown in Fig. 4. The Yb clock has a stability of $\sigma(\tau) = 1.4 \times 10^{-16}/\sqrt{\tau}$; therefore, a measurement of the $\nu_{\mathrm{Al}^+}/\nu_{\mathrm{Yb}}$ frequency ratio provides a direct measure of the $^{27}Al^+$ clock stability [8, 37]. The $^{27}Al^+$ clock beam pathlengths are stabilized from the output of the UV frequency doubler to the vacuum chamber [38] and the probe time of 150 ms is chosen to optimize the stability. The asymptotic stability is fit to $\sigma(\tau) = 1.2 \times 10^{-15}/\sqrt{\tau}$, consistent with the expected quantum projection noise [41]. In the future, it should be possible to increase the probe time to achieve a single

ion clock stability near $10^{-16}/\sqrt{\tau}$ with the use of a more stable clock laser [42].

In conclusion, we have developed an $^{27}Al^+$ quantum-logic clock with a total systematic uncertainty of $\Delta\nu/\nu = 9.4 \times 10^{-19}$, fulfilling the vision of Dehmelt that a "mono-ion oscillator" achieve a systematic uncertainty of 10^{-18}. The systematic uncertainty is limited by the uncertainty in the time-dilation shift due to excess micromotion. Further improvements in trap design, uncertainty in the static differential polarizability, and a reduction in background gas pressure may lead to an improvement in the systematic uncertainty of the clock.

We thank T. Rosenband for development of the initial version of the ion trap used for this clock and useful discussions. We thank K. Beloy and J. Bergquist for useful discussions, A. Ludlow, W. McGrew, and X. Zhang for operating the Yb lattice clock, S. Diddams, T. Fortier, and H. Leopardi for frequency measurements, and J. Bollinger and C. Oates for their careful reading of the manuscript. This work was supported by the National Institute of Standards and Technology, the Defense Advanced Research Projects Agency, and the Office of Naval Research. S.M.B. was supported by the U.S. Army Research Office through MURI Grant No. W911NF-11-1-0400. This Letter is a contribution of the U.S. Government, not subject to U.S. copyright.

* samuel.brewer@nist.gov
† Current Address: IonQ, Inc., College Park, MD 20740
‡ Current Address: Honeywell Quantum Solutions, Broomfield, CO 80021
§ david.leibrandt@nist.gov

[1] H. G. Dehmelt, Bulletin of the American Physical Society **18**, 1521 (1973).
[2] H. G. Dehmelt, Bulletin of the American Physical Society **20**, 60 (1975).
[3] D. J. Wineland and H. G. Dehmelt, Bulletin of the American Physical Society **20**, 637 (1975).
[4] H. G. Dehmelt, IEEE Trans. Instrum. Meas. **IM-31**, 83 (1982).
[5] M. S. Safronova, D. Budker, D. DeMille, D. F. Jackson Kimball, A. Derevianko, and C. W. Clark, Rev. Mod. Phys. **90**, 025008 (2018).
[6] F. Riehle, P. Gill, F. Arias, and L. Robertsson, Metrologia **55**, 188 (2018).
[7] H. Denker, L. Timmen, C. Voigt, S. Weyers, E. Peik, H. S. Margolis, P. Delva, P. Wolf, and G. Petit, Journal of Geodesy **92**, 487 (2018).
[8] W. F. McGrew, X. Zhang, R. J. Fasano, S. A. Schäffer, K. Beloy, D. Nicolodi, R. C. Brown, N. Hinkley, G. Milani, M. Schioppo, T. H. Yoon, and A. D. Ludlow, Nature **564**, 87 (2018).
[9] C. W. Chou, D. B. Hume, J. C. J. Koelemeij, D. J. Wineland, and T. Rosenband, Phys. Rev. Lett. **104**, 070802 (2010).
[10] T. L. Nicholson, S. L. Campbell, R. B. Hutson, G. E. Marti, B. J. Bloom, R. L. McNally, W. Zhang, M. D. Barrett, M. S. Safronova, G. F. Strouse, W. L. Tew, and J. Ye, Nature Communications **6**, 6896 (2015).
[11] A. D. Ludlow, M. M. Boyd, J. Ye, E. Peik, and P. O. Schmidt, Rev. Mod. Phys. **87**, 637 (2015).
[12] N. Huntemann, C. Sanner, B. Lipphardt, C. Tamm, and E. Peik, Phys. Rev. Lett. **116**, 063001 (2016).
[13] M. Schioppo, R. C. Brown, W. F. McGrew, N. Hinkley, R. J. Fasano, K. Beloy, T. H. Yoon, G. Milani, D. Nicolodi, J. A. Sherman, N. B. Phillips, C. W. Oates, and A. D. Ludlow, Nature Photonics **11**, 48 (2017).
[14] E. Oelker, R. B. Hutson, C. J. Kennedy, L. Sonderhouse, T. Bothwell, A. Goban, D. Kedar, C. Sanner, J. M. Robinson, G. E. Marti, D. G. Matei, T. Legero, M. Giunta, R. Holzwarth, F. Riehle, U. Sterr, and J. Ye, arXiv e-prints , arXiv:1902.02741 (2019), arXiv:1902.02741 [physics.atom-ph].
[15] T. Rosenband, D. B. Hume, P. O. Schmidt, C. W. Chou, A. Brusch, L. Lorini, W. H. Oskay, R. E. Drullinger, T. M. Fortier, J. E. Stalnaker, S. A. Diddams, W. C. Swann, N. R. Newbury, W. M. Itano, D. J. Wineland, and J. C. Bergquist, Science **319**, 1808 (2008).
[16] J.-S. Chen, S. M. Brewer, C. W. Chou, D. J. Wineland, D. R. Leibrandt, and D. B. Hume, Phys. Rev. Lett. **118**, 053002 (2017).
[17] J.-S. Chen, Ph.D. thesis, University of Colorado, Boulder (2017).
[18] See Supplemental Material [url] for additional details on the experimental setup and motional and blackbody radiation frequency shift evaluations, which includes Refs. [19-24].
[19] J. Keller, *Spectroscopic characterization of ion motion for an optical clock based on Coulomb crystals*, Ph.D. thesis, Gottfried Willhelm Leibniz Universitat, Hannover (2015).
[20] T. F. Gallagher and W. E. Cooke, Phys. Rev. Lett. **42**, 835 (1979).
[21] W. M. Itano, L. L. Lewis, and D. J. Wineland, J. de Phys. **Colloque C8**, 283 (1981).
[22] W. M. Itano, L. L. Lewis, and D. J. Wineland, Phys. Rev. A **25**, 1233(R) (1982).
[23] S. G. Porsev and A. Derevianko, Phys. Rev. A **74**, 020502(R) (2006).
[24] T. Rosenband, W. M. Itano, P. O. Schmidt, D. B. Hume, J. C. J. Koelemeij, J. C. Bergquist, and D. J. Wineland, in *Proc. EFTF Conf.* (2006) p. 289.
[25] P. O. Schmidt, T. Rosenband, C. Langer, W. M. Itano, J. C. Bergquist, and D. J. Wineland, Science **309**, 749 (2005).
[26] D. B. Hume, T. Rosenband, and D. J. Wineland, Phys. Rev. Lett. **99**, 120502 (2007).
[27] T. Rosenband, P. O. Schmidt, D. B. Hume, W. M. Itano, T. M. Fortier, J. E. Stalnaker, K. Kim, S. A. Diddams, J. C. J. Koelemeij, J. C. Bergquist, and D. J. Wineland, Phys. Rev. Lett. **98**, 220801 (2007).
[28] D. J. Berkeland, J. D. Miller, J. C. Bergquist, W. M. Itano, and D. J. Wineland, J. Appl. Phys. **83**, 5025 (1998).
[29] J. Keller, H. L. Partner, T. Burgermeister, and T. E. Mehlstäubler, J. Appl. Phys. **118**, 104501 (2015).
[30] H. C. J. Gan, G. Maslennikov, K.-W. Tseng, T. R. Tan, R. Kaewuam, K. J. Arnold, D. Matsukevich, and M. D. Barrett, Phys. Rev. A **98**, 032514 (2018).
[31] S. M. Brewer, J. S. Chen, K. Beloy, A. M. Hankin, E. R. Clements, C. W. Chou, W. F. McGrew,

X. Zhang, R. J. Fasano, D. Nicolodi, H. Leopardi, T. M. Fortier, S. A. Diddams, A. D. Ludlow, D. J. Wineland, D. R. Leibrandt, and D. B. Hume, arXiv e-prints , arXiv:1903.04661 (2019).

[32] F. Diedrich, J. C. Bergquist, W. M. Itano, and D. J. Wineland, Phys. Rev. Lett. **62**, 403 (1989).

[33] C. Monroe, D. M. Meekhof, B. E. King, S. R. Jefferts, W. M. Itano, D. J. Wineland, and P. Gould, Phys. Rev. Lett. **75**, 4011 (1995).

[34] M. S. Safronova, M. G. Kozlov, and C. W. Clar, Phys. Rev. Lett. **107**, 143006 (2011).

[35] A. M. Hankin, E. R. Clements, Y. Huang, S. M. Brewer, J. S. Chen, C. W. Chou, D. B. Hume, and D. R. Leibrandt, arXiv e-prints , arXiv:1902.08701 (2019).

[36] K. Beloy, D. R. Leibrandt, and W. M. Itano, Physical Review A **95**, 043405 (2017).

[37] M. Schioppo, R. C. Brown, W. F. McGrew, N. Hinkley, R. J. Fasano, K. Below, T. H. Yoon, G. Milani, D. Nicolodi, J. A. Sherman, N. B. Phillips, C. W. Oates, and A. D. Ludlow, Nature Photonics **11**, 48 (2016).

[38] L. S. Ma, P. Jungner, J. Ye, and J. L. Hall, Opt. Lett. **19**, 1777 (1994).

[39] C. W. Chou, D. B. Hume, M. J. Thorpe, D. J. Wineland, and T. Rosenband, Phys. Rev. Lett. **106**, 160801 (2011).

[40] D. B. Hume and D. R. Leibrandt, Phys. Rev. A **93**, 032138 (2016).

[41] W. M. Itano, J. C. Bergquist, J. J. Bollinger, J. M. Gilligan, D. J. Heinzen, F. L. Moore, M. G. Raizen, and D. J. Wineland, Phys. Rev. A **47**, 3554 (1993).

[42] D. G. Matei, T. Legero, S. Häfner, C. Grebing, R. Weyrich, W. Zhang, L. Sonderhouse, J. M. Robinson, J. Ye, F. Riehle, and U. Sterr, Phys. Rev. Lett. **118**, 263202 (2017).